



OPEN Investigating hepatic fibrosis heterogeneity by three-dimensional imaging in metabolic dysfunction-associated steatotic liver disease

Buket Yigit¹, Ekin Ozgonul², Omer Yaman², Tarik Sipahioglu¹, Burge Ulukan¹, Yagmur Cetin Tas³, Berna Morova², Musa Aydin⁴, Yigit Uysalli², Elif Demirtas⁵, Mert Erkan⁶, Gurkan Tellioglu⁷, Dila Atak³, Yasemin Gursoy Ozdemir³, Sercin Karahuseyinoglu⁸, Cihan Yurdaydin¹, Murat Akyildiz¹, Abhishek Sheth⁹, Guruprasad Padur Aithal⁹, Hale Kirimlioglu¹⁰, Murat Dayangac¹¹, Onur Ferhanoglu¹², Alper Kiraz² & Müjdat Zeybel¹✉

Although liver biopsy is a well-established technique to assess fibrosis it has several limitations, including invasive nature, semi-quantitative assessment methods, significant sampling and observer variability, making precise assessment of hepatic fibrosis challenging. Accurate and reliable modalities are crucial for clinical trials to characterize hepatic fibrosis monitorization effectively. We aimed to perform 3-dimensional imaging of optically transparent liver samples by light-sheet microscopy (LSM) to quantify extracellular matrix (ECM) proteins. Fifty-seven MASLD, thirty-eight chronic hepatitis patients and twelve healthy individuals were included. Liver tissues were cleared with a CLARITY method. 3D imaging of ECM was performed via the newly developed LSM. Collagen Proportionate Volume (CPV) and Elastin Proportionate Volume (EPV) values were calculated by analysis of over 200 sections per sample through morphometry. We have optimized a method which achieves transparency of liver tissues in advanced fibrotic stages of MASLD and optimized non-destructive slide-free fibrosis pathology of whole fresh and FFPE liver biopsy samples. Cut-off values for CPV and EPV were established for fibrotic stages. CPV and EPV analysis showed a considerable optical section heterogeneity resulting in a fibrosis stage of variance within the sample. Volumetric image analysis for fibrosis staging revealed that only 44% and 47% of optical sections would be staged the same for F3 and F4, respectively. For the first time, our findings demonstrate a novel method of analyzing 3D digital pathology of liver fibrosis using in-house LSM. Volumetric imaging of whole liver biopsy samples showed that fibrosis heterogeneity occurs even in different sections.

Keywords Liver fibrosis, Slide-free pathology, CLARITY, 3D imaging, MASLD

Liver fibrosis is an aberrant wound healing response to repetitive hepatic injury, which culminates in replacement of healthy liver parenchyma with extracellular matrix (ECM) proteins. It refers to the common final stage of any chronic liver disease, regardless of its cause. Chronic deposition of fibrillar ECM components

¹Department of Gastroenterology and Hepatology, School of Medicine, Koç University, Istanbul 34010, Turkey. ²Department of Physics, Koç University, Istanbul 34450, Turkey. ³Department of Neuroscience, School of Medicine, Koç University, Istanbul 34010, Turkey. ⁴Department of Computer Engineering, Fatih Sultan Mehmet Vakif University, Istanbul 34083, Turkey. ⁵Graduate School of Health Sciences, Koç University, Istanbul 34010, Turkey. ⁶Department of General Surgery, Faculty of Medicine, Acibadem University, Istanbul 34752, Turkey. ⁷Department of General Surgery, School of Medicine, Koç University, Istanbul 34010, Turkey. ⁸Department of Histology and Embryology, School of Medicine, Koç University, Istanbul 34010, Turkey. ⁹Nottingham University Hospitals NHS Trust & University of Nottingham, NIHR Nottingham Biomedical Research Centre, Nottingham NG7 2UH, UK. ¹⁰Department of Pathology, Faculty of Medicine, Acibadem University, Istanbul 34752, Turkey. ¹¹Department of General Surgery, Faculty of Medicine, Medipol University, Istanbul 34214, Turkey. ¹²Department of Electronics and Communication Engineering, Istanbul Technical University, Istanbul 34467, Turkey. ✉email: mzeybel@ku.edu.tr

leads to complex tissue remodelling based on the balance between mechanisms of fibrogenesis and fibrolysis¹. Metabolic dysfunction-associated steatotic liver disease (MASLD) prevalence is on the rise and becoming the most common cause of chronic liver disease worldwide, reflecting the burgeoning global prevalence of diabetes and obesity². Although approximately one third of adults have MASLD, only a small proportion of patients have advanced disease associated with fibrosis³. Hepatic fibrosis is the major predictor of morbidity and mortality in MASLD^{4,5}. The prevalence and association between MASLD and fibrosis is relatively well-established, however, this varies significantly according to the genetic variants (*PNPLA3*, *TM6SF2*), body mass index (lean or obese individuals), and diabetes^{6,7}. Specialist care is largely devoted to advanced fibrosis, therefore, precise assessment of hepatic fibrosis is a prerequisite for healthcare allocation, biomarker and drug development in the era of MASLD clinical trials.

The presence of hepatic fibrosis represents a key histopathological parameter for the determination of disease severity and subsequent therapeutic decisions. This is why liver biopsy has been the most reliable method of evaluating hepatic fibrosis for many decades. Liver biopsy is not a perfect tool and does carry some flaws. Fibrosis staging relies on semi-quantitative scoring which exhibits a non-linear relationship between the stage and content of fibrosis^{8,9}. Variability in the interpretation of core biopsy specimens is considerable, leading to poor reliability of hepatic fibrosis staging^{10,11}. Several studies, including a paired biopsy study, have highlighted substantial sampling variability¹². Sampling error and observer variability result in considerable diagnostic and staging inaccuracies, which are a major limitation for the success of MASLD clinical trials¹³. In an attempt to address these challenges, several studies have developed novel methods of improving histological examination. These include computerized image analysis and second harmonic generation microscopy. Morphometric image analysis provides the quantification of picrosirius red-stained hepatic scarring by measuring a collagen proportionate area (CPA)¹⁴. Evidence shows CPA performs better than standard scoring in correlating with hepatic venous pressure and predicting hepatic decompensation^{15,16}. Multiphoton microscopy by second harmonic generation (SHG) presented a tool for quantifying fibrillar collagen in liver slices¹⁷. A dual-photon microscopy-based method further provides improved accuracy of hepatic fibrosis quantification¹⁸. A recent study investigated three dimensional analysis of cleared human liver tissues by multiphoton microscopy¹⁹. This study demonstrated spatially distributed morphological changes in early stages of MASLD. To date, three-dimensional imaging of clinical liver specimens beyond 60- μm of depth has not been reported.

A comprehensive understanding of hepatic ECM remodelling may be improved by spatial resolution imaging in three dimensions, however, imaging of large tissues such as core biopsies is a particularly difficult task. Biopsy specimens initially need to be processed into a transparent form to minimize light scattering to achieve optimal deep optical imaging²⁰. Light scattering can be reduced by advanced tissue clearing techniques such as CLARITY, CUBIC and iDISCO. Imaging of the large tissue specimens can be only achieved by cutting-edge optical systems enabling rapid high-quality imaging^{21–23}. The above-mentioned methods use different clearing agents, resulting in cleared tissue with distinct refractive indices. In the CLARITY method, sodium dodecyl sulfate (SDS) serves as a clearing agent, helping to remove phospholipids from the cell membrane, while the monomer solution preserves the tissue structure. CUBIC involves strong chemicals and urea and dimethylformamide (DMF) as a clearing agent and has been used for large biological samples. iDISCO method combines dichloromethane and methanol for clearing and is designed to visualize large and intact biological samples. Several optical approaches have been developed to visualize large intact tissues, including confocal and multi-photon microscopy. Penetration depth of such techniques is typically a maximum of 300- μm and is associated with slow recording and substantial photo-bleaching problems²⁴. Another notable method is light-sheet microscopy (LSM), which permits high-speed imaging of optically cleared tissues by only illuminating the detection plane. To the best of our knowledge, tissue clarification approaches and LSM previously have not been tested in significantly scarred tissues.

In this study, we sought to accurately characterize multi-slice ECM remodelling throughout liver tissues by enhancing tissue transparency using the CLARITY technique. We established a precise LSM-based 3D digital pathology platform to perform volumetric fibrosis imaging of whole liver biopsy specimens. The application of automated code in slide-free non-destructive pathology provided efficient and effective quantification of multiple ECM components when compared to traditional liver biopsy analysis (Fig. 1).

Results

To demonstrate the capability of our 3D imaging platform for visualizing ECM components, we prospectively recruited fifty-seven patients with biopsy-proven MASLD (Supplementary Table 1). We further included twelve patients who underwent hepatic resection due to benign and malignant liver diseases without any parenchymal diseases into the study (Supplementary Table 2). Demographic and laboratory characteristics along with histopathological stages are shown in Supplementary Tables 1 and 2. We first explored the volumetric distribution of the most abundant ECM protein of collagen type I across fibrotic stages of MASLD (Fig. 2). The hepatic content of elastin was subsequently explored with fluorescence staining (Fig. 3). Collagen type I and elastin expressions were detected in perisinusoidal, periportal, bridging and nodular patterns as gradually increasing in fibrotic stages. We observed higher expression of both proteins in advanced fibrotic stages of MASLD as expected. 2-dimensional sections were reconstructed into 3D volume as shown in movie S1-8 (<https://data.mendeley.com/datasets/hk2zdg674r/draft?a=bb1dd448-bedc-4713-ae28-8f55e2e2d0f6>). While volumetric imaging of collagen type I and elastin enabled appreciation of fibrosis patterns in advanced fibrotic stages of MASLD, visualization of several planes highlighted substantially heterogeneous distribution of fibrosis. This sectional variability could potentially lead to misclassification of patients. Indeed here, we identified six discordant cases out of 56 patients who underwent liver transplantation due to decompensated chronic liver disease despite the pathological assessment of explant livers revealed only bridging fibrosis. Furthermore, staging in different planes of the specimen by an expert pathologist revealed stage 2, 3 and 4 fibrosis as presented in Fig. 4A.

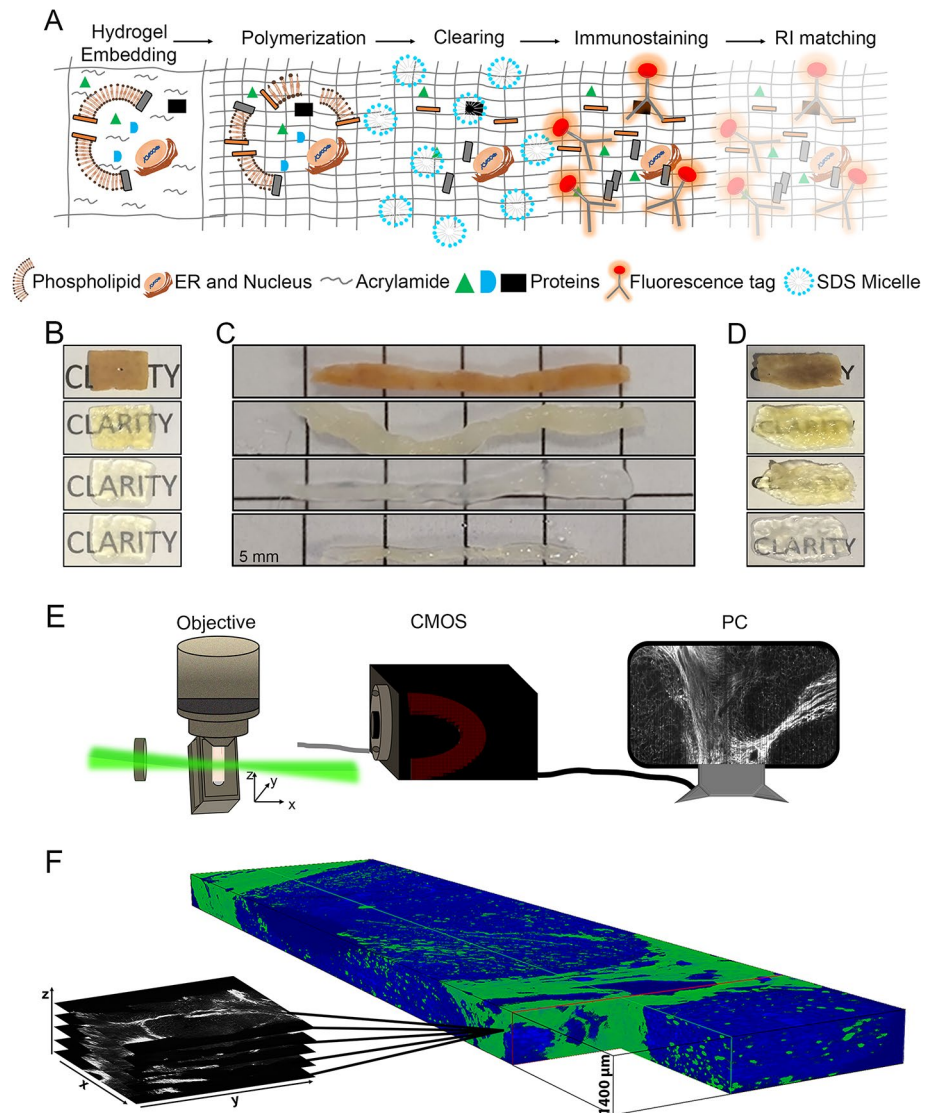


Fig. 1. A summary of 3D imaging in cleared liver tissues. **(A)** The illustration represents the CLARITY method using **(B)** a non-fibrotic liver tissue, **(C)** a core liver biopsy, and **(D)** a cirrhotic liver tissue. **(E)** Macro configuration of in-house developed LSM and **(F)** stack image show 3D reconstruction in cleared liver tissue stained against Collagen type I. (Coll-1: Collagen type I; Green, nuclei: Blue) CMOS; Complementary metal-oxide-semiconductor, LSM; Light sheet microscopy. 3D image was created using Leica Application Suite X (Version 3.5.5.19976, URL: <https://www.leica-microsystems.com/products/microscope-software/p/leica-las-x-ls/>).

Quantification of ECM components in whole core biopsies and introduction of CPV and EPV

These results demonstrate that 3D slide-free histopathological analysis may be a promising tool for fibrosis assessment. Apart from obtaining volumetric images, this observation indicates the requirement for precise measurement of scarring across all planes of the specimen. In aid of this, we developed a multi-sectional ECM quantification platform based on a computer-assisted morphometric analysis of whole core liver biopsy specimens (typically with a diameter and length of 1.4 mm by 2 cm). As shown in Supplementary Fig. S1, images were stitched and ECM proportionate area analysis was performed by a designed macro code throughout the steps of contrast enhancement of raw images, binarization of enhanced images, thresholding, and area measurement. The whole liver section area was determined by the Huang thresholding algorithm, while the total collagen-stained area was determined by the Otsu thresholding algorithm likewise previously published methods (Supplementary Fig. S1). Finally, collagen proportionate area (CPA) was determined as a ratio of collagen-stained area to whole specimen area similar to previously published methods¹⁵. Of note, the ECM quantification platform analyzed the entire sections obtained from a specimen, which included 100–400 sections per sample (mean \pm SD: 197 ± 99) rather than a single section CPA analysis as in the conventional method. The peak fibrosis CPA values were clustered at 0–4% for F0, 0–12% for F1, 6–15% for F2, 10–25% for F3 and 15–30% for cirrhosis (Fig. 4B–F). However, the 3D histogram analysis revealed a wide range of collagen type I intensities within the

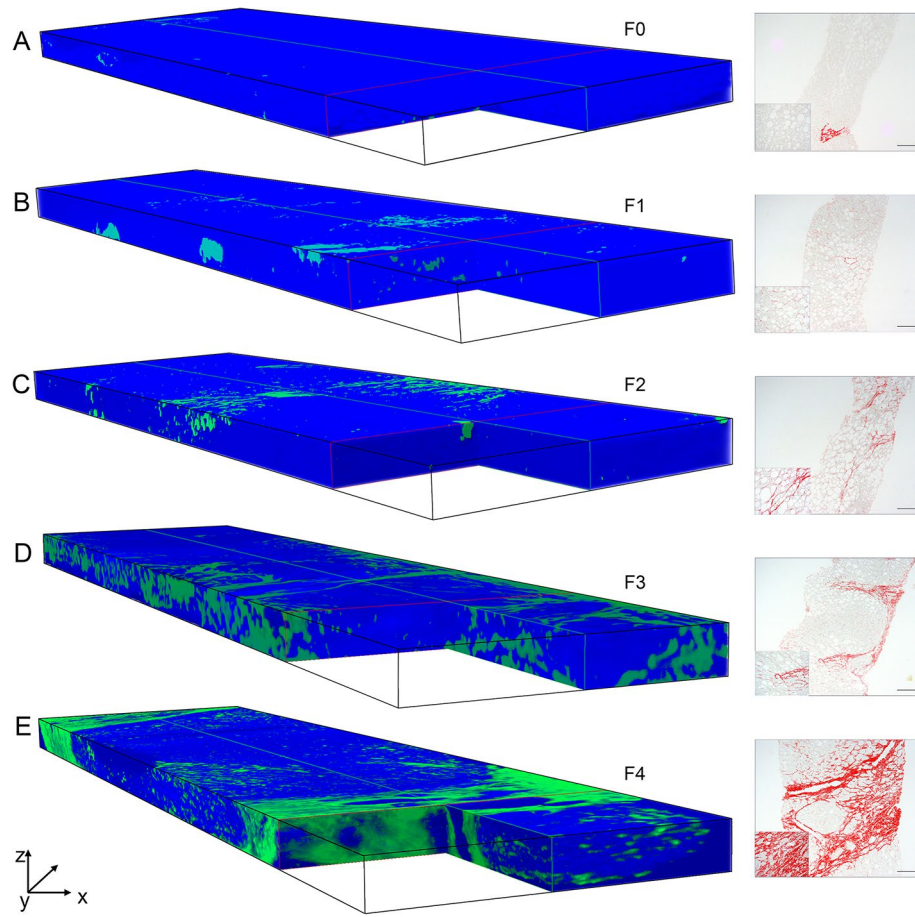


Fig. 2. Collagen type I staining in cleared liver tissue. 3D images represent a part of the whole liver tissue stained with Coll-1 antibody. Digital pathological assessment shows more pronounced fibrillar staining as the disease progresses (A) F0, (B) F1, (C) F2, (D) F3, and (E) F4 in MASLD. Coll-1 antibody specificity is compared with its corresponding 2D histological liver sections (right). (Coll-1: Collagen type I; Green, nuclei; Blue, scale bar: 200 μm , left-bottom images are captured with a 40X magnification). 3D images were created using Leica Application Suite X (Version 3.5.5.19976, URL: <https://www.leica-microsystems.com/products/microscope-software/p/leica-las-x-ls/>).

fibrosis stage suggesting three-dimensional heterogeneity of ECM components (Fig. 4G). Additionally, CPV or EPV values significantly changed across fibrosis stages ($p < 0.01$ for CPV, $p < 0.01$ for EPV). Similar analysis for the HFHS and CCl4 model demonstrated less variability of collagen type I in liver tissues (Supplementary Fig. S2). We repeated a similar analysis of whole liver specimens for elastin staining (Supplementary Fig. S3). Peak Elastin Proportionate Area (EPA) intensities were clustered at 0–6% for F0, 0–10% for F1, 0–20% for F2, 15–25% for F3 and 15–30% for cirrhosis. 3D ECM components most prominently showed overlapping intensities in F3 and F4 fibrosis stages.

We implemented the 3D analysis of collagen proportionate volume (CPV) and elastin proportionate volume (EPV); which represents the mean of CPA and EPA measurements per specimen, respectively. Measurement of spread is provided with interquartile range in Fig. 5A and D. Subsequently, coefficient of variation analysis was performed to determine extent of variability. Interestingly, approximately 85% of CPV and EPV samples demonstrated intermediate or high coefficient of variation underlining the significance of sectional variation (Fig. 5B and E). We optimized the cut-offs for collagen type I-based CPA, CPV and EPV to establish the basis for three-dimensional fibrosis staging. AUROC curve and Youden index analysis differentiated fibrosis stages which determined $4.3 \leq F1 \leq 8.7$, $8.7 < F2 \leq 17.7$, $17.7 < F3 \leq 24.7$ and $24.7 < F4$ cut-offs for CPV and $5.4 \leq F1 \leq 9.8$, $9.8 < F2 \leq 16.6$, $16.6 < F3 \leq 26.9$ and $26.9 < F4$ cut-offs for EPV (Fig. 5C, F). We performed CPV and EPV analysis for 6 patients who underwent liver transplantation with histopathological diagnosis of bridging fibrosis. This analysis indicated CPV of $28.3 \pm 3.9\%$ (mean \pm SD) and EPV of $24.9 \pm 3.4\%$ (mean \pm SD) suggestive of cirrhosis with the new assessment method.

To further explore whether CPV and EPV assessment would show diagnostic concordance with 2D histopathological staging, we generated 3D histograms which showed a percentage of slices according to adjusted CPV and EPV cut-off values. These results indicated the significant peaks of ECM components in relevant fibrotic stages; however, a significant number of slices would be classified in the higher or lower fibrosis

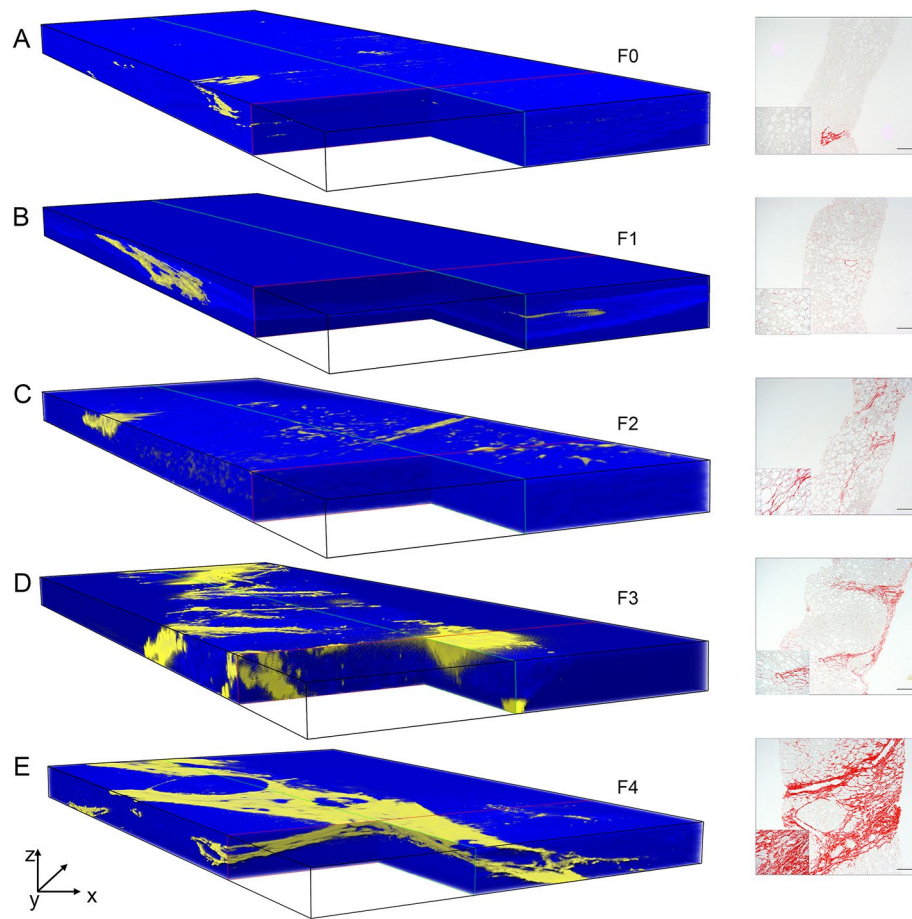


Fig. 3. Elastin staining in cleared liver tissue. 3D representative images from a part of the whole liver tissue (left) show intense Elastin staining in fibrotic areas as the disease progresses (A) F0, (B) F1, (C) F2, (D) F3, and (E) F4 and histological assessment is compared with its corresponding 2D Sirius Red staining (right). (Elastin: Yellow, Nuclei: Blue, scale bar: 200 μm , left-bottom images are captured with a 40X magnification). 3D images were created using Leica Application Suite X (Version 3.5.5.19976, URL: <https://www.leica-microsystems.com/products/microscope-software/p/leica-las-x-ls/>).

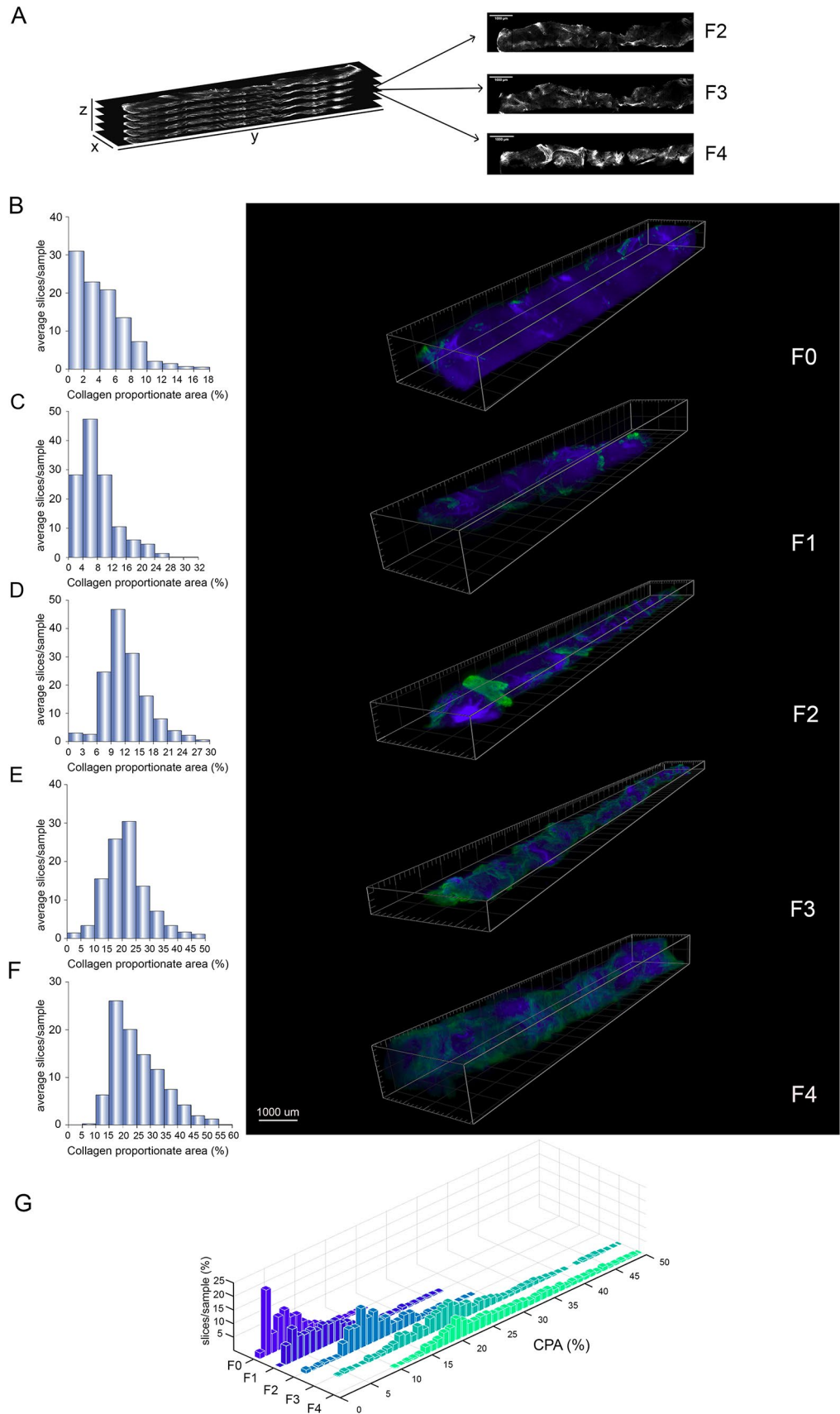
stages (Fig. 5G and H). For instance, only 44% of the optical sections for the F3 patients and 47% of the sections for the F4 patients would be classified in the same stage according to volumetric analysis.

To determine whether the observed sectional variability is unique to MASLD, further analysis was carried out in viral hepatitis-related chronic liver disease. We optically cleared forty-one liver specimens and performed CPV and EPV analysis (Supplementary Table 3). Despite a tendency towards a more prominent heterogeneity of CPV values in the MASLD cohort compared to viral hepatitis, this difference was not statistically significant (Supplementary Fig. S4). However, EPV coefficient of variation of MASLD was higher compared to viral hepatitis-related chronic liver disease (Supplementary Fig. S4).

Further to demonstrate the clinical applicability of 3D slide-free histopathological fibrosis analysis, we deparaffinized and optically cleared FFPE liver specimens ($n = 10$). Both non-fibrotic and advanced fibrotic MASLD samples were passively clarified and full transparency was achieved similar to fresh tissue samples. Peak EPV intensities were clustered at 0–9% for F0 and 14–25% for cirrhosis in line with fresh specimens.

Discussion

Accurate evaluation of liver fibrosis and ECM remodelling in liver samples remains an important issue^{25,26}. A recent study indicated a particularly low reliability of histopathological fibrosis staging in MASLD, highlighting the unmet need for more precise methods¹¹. Given biopsy samples are not fully utilized for clinical decisions, here, we demonstrate how our platform via combining two cutting-edge approaches (CLARITY and LSM) enables precise three-dimensional optical imaging of liver specimens. State-of-the-art clearing techniques, light-sheet microscopy and a large cohort of patients with clarified liver samples allowed us to investigate 3D volumetric imaging of hepatic fibrosis. As commercially available light sheet microscopes are not designed to visualize biopsy specimens, we constructed a custom-made light sheet microscope. This approach has successfully mapped major fibrosis components of scarring, collagen type I and elastin, across liver tissues and core liver



biopsies. Equally, this study shows, for the first time, advanced scarring is not a limitation for volumetric imaging at least for chronic liver diseases.

An interesting finding is the observation of substantial inter-sectional variability of hepatic fibrosis within a sample. This study extends previous paired biopsy and MR elastography-based investigations demonstrating

Fig. 4. Imaging of CLARITY-processed intact liver biopsy reveals extensive fibrosis heterogeneity between optical sections in MASLD. **(A)** Three different optical sections obtained from an intact liver biopsy sample are evaluated and assessed with a different fibrosis stage by an expert pathologist. Whole liver biopsies from different stages of liver fibrosis **(B)** F0, **(C)** F1, **(D)** F2, **(E)** F3 and **(F)** F4 are stained with Collagen type I without histological sectioning. **(B–F)** Histogram analysis shows the average distribution in optical sections per whole biopsy sample using CPA approach. **(G)** 3D histogram analysis shows the percentage of optical sections per whole biopsy sample in fibrosis groups and emphasizes the overlap between F3 and F4 stage. (CPA: Collagen proportionate area). 3D images were created using Imaris Viewer (Version 10.1.0, URL: <https://imaris.oxinst.com/imaris-viewer>).

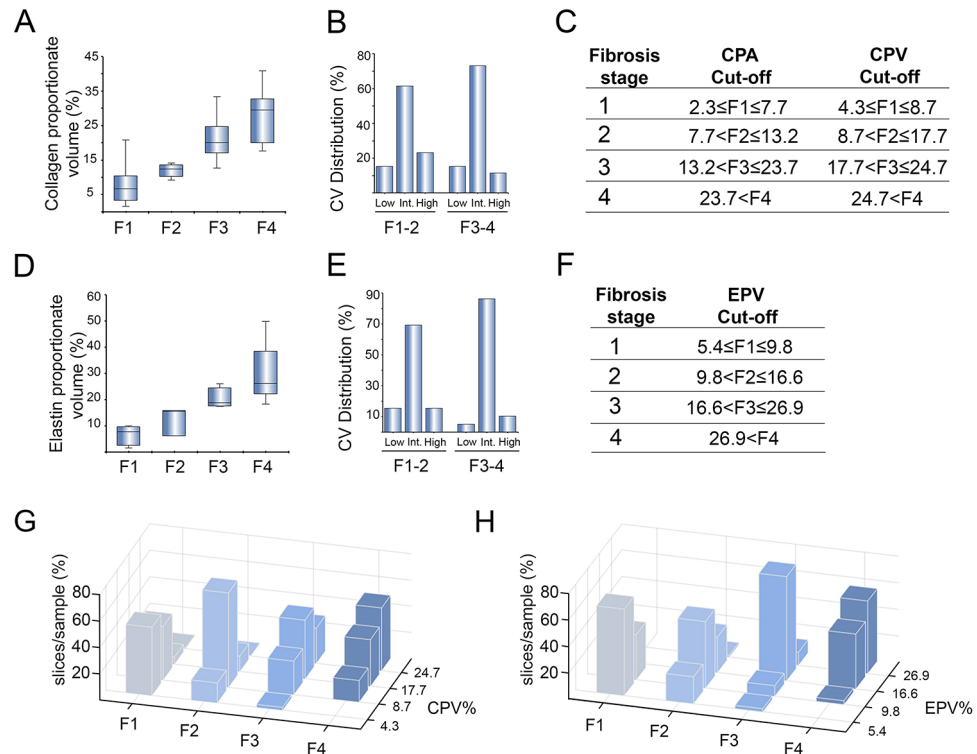


Fig. 5. F3-4 MASLD fibrosis groups have significantly higher fibrosis heterogeneity than F1-2. **(A)** IQR is calculated for each fibrosis group and indicates a larger distribution of CPV values in F3-4. **(B)** Obtained values from CV analysis per sample is used to determine the cut-off values. The variation degree of each sample in F1-2 and F3-4 is stated according to the cut-off values. **(C)** Cut-off values are determined from the AUROC for CPA and CPV based on the Youden index. **(D)** IQR is calculated for each group and indicates a larger distribution of EPV values in F3-4. **(E)** Obtained values from CV analysis per sample are used to determine the cut-off values of EPV. The variation degree of each sample in F1-2 and F3-4 is stated according to the EPV cut-off values. **(F)** Cut-off values are determined from the AUROC for EPV based on the Youden index. **(G and H)** The 3D histogram analysis executed in MATLAB shows the percentage of slices based on CPV and EPV cut-off values in fibrosis stages. CV: Coefficient of variation; IQR: interquartile range; $*p < 0.05$, $**p < 0.01$, $***p < 0.001$. Int: intermediate.

uneven distribution of liver fibrosis by showing this variability exists even between the 2 μm thick planes of the specimen^{12,27}. Our approach provided continuous volumetric measurements of fibrosis organisation of whole samples. Heterogeneity of fibrosis measurements within the fibrotic stages was remarkable which could be associated with discordance between histology and severity of liver disease. We hereby show the slide-free 3D pathology provides higher resolution of fibrosis composition; resulting in less than 50% of sectional concordance in F3 and F4 stages. In line with our results, a previous MR elastography-based study reported mean variability of 30.59% in liver stiffness which suggests pathological scoring can overestimate or underestimate fibrosis stage depending on the fibrosis heterogeneity²⁷. Similarly, another study also reported that over 45% of the patients had at least one stage higher liver stiffness than reported mean liver stiffness in one fifth of the liver parenchyma²⁸. Observation of inconsistencies between the histopathological fibrosis staging and clinical outcomes in MASLD is not uncommon. Sanyal et al. reported a remarkably high rate of progression from bridging fibrosis to cirrhosis in a relatively short clinical trial of 29 months²⁹. Fibrosis progression rate varies between individuals and true rapid clinical progression cannot be ruled out. However, it is also possible that sampling error is the main culprit here leading to histopathological discordance. Our work illustrates how volumetric assessment of collagen

elastin (CPV and EPV) can improve accurate staging of hepatic fibrosis. Based on our analysis, we defined the CPV cut-offs as 4.3, 8.7, 17.7, and 24.7 for F1, F2, F3 and F4, respectively. The cut-off values determined in the current study will be the basis for the development of 3D fibrosis staging. Further studies in larger populations and different patient groups are required to determine the effectiveness of this method.

The major advantage of non-destructive volumetric pathology is the ability to obtain whole specimen imaging without sectioning. Slide-based histological examination is frequently associated with fragmentation leading to difficulty of portal area assessment in advanced fibrotic stages³⁰. On the other hand, our slide-free approach allows assessment of more portal triads. Recent studies have successfully applied this technique for prostate and breast core biopsy samples³¹. Given this technique has been successful in formalin-fixed and paraffin-embedded (FFPE) and significantly fibrotic specimens in this study, 3D digital pathology can enhance the use of archival FFPE clinical specimens with a potential to revolutionise the optical imaging of clinical specimens^{32,33}. Review of paired liver biopsy samples from MASH clinical trials via 3D fibrosis pathology could be of value in better understanding clinical trials where negative outcomes are often due to failure in fibrosis reduction¹³. At present, our approach could only map ECM components. Future applications include 3D fluorescent haematoxylin and eosin-like images which would be able to examine steatosis, inflammation and ballooning degeneration³⁴. Of value is the potential use of any remaining tissue in omics studies, since fixation and clearing steps leave the majority of nucleic acids and proteins intact. Our study shows potential for liver tissue clearing and 3D ECM imaging as a powerful tool for precise fibrosis staging and monitoring/accurate stratification of chronic liver disease activity. Given the high fibrosis heterogeneity of ECM components in liver specimens, there is a potential for broad application in diverse etiologies. Instead of relying on existing single-section based histopathological examination, 3D pathology of whole liver biopsy samples can be used on archived biopsies of clinical trials and future examinations. In addition, slide-free 3D pathology could offer a diagnostic and prognostic opportunity, particularly in high-risk individuals for fibrosis progression.

By only focussing on major fibrillar ECM components; collagen I and elastin, this study is not without limitations. Other ECM components including fibronectin, laminin and integrins may have different patterns of distribution and need to be studied in further volumetric studies if our findings of collagen type I and elastin are universal for fibrosis. Moreover, CPV and EPV cut-offs were based on a relatively small cohort size for the F1 and F2 stages. We included a modest cohort of 110 patients for this proof-of-concept study. A larger cohort size would be needed to revalidate cut-offs for further 3D pathology studies. Another potential limitation includes the lack of MR elastography and vibration-controlled transient elastography-based liver stiffness data and comparison with histopathological examination and 3D fibrosis examination. To further establish this method as a diagnostic tool, it will be essential to have MR elastography data. The prognostic value could also be examined in a cohort of F3 and F4 patients with hepatic venous pressure gradient measurements. This information could be able to confirm histopathological misdiagnosis for cirrhotic patients.

In summary, we envision the application of tissue clarification and LSM to acquire fluorescent signals from liver specimens in facilitating spatial resolution imaging. Here we demonstrated substantial variability of hepatic fibrosis in optical sections of specimens. For the first time, we provided an alternative approach of volumetric ECM assessment to overcome discordance between histopathological examination and clinical severity of chronic liver disease. To develop potential anti-fibrotic therapies, it is crucial to quantify and record the dynamics of fibrosis in different regions of the liver. Given the exponential increase in MASLD clinical trials, this platform can be a corner stone for precise monitoring of hepatic fibrosis and other pathologies in hepatology. Several promising directions for future work can be generated to have applications beyond fibrosis. These applications include three-dimensional assessment of necrosis, apoptosis, ballooning hepatocytes, immune cells and myofibroblasts. The application of this method may have broader research implications such as 3D investigation of cellular interactions in chronic liver disease and hepatocellular carcinoma. We anticipate 3D digital pathology is a promising tool for investigating complex liver pathologies with considerable heterogeneity.

Methods

Patient materials

Liver samples with various stages of fibrosis were collected from patients with MASLD and chronic hepatitis B, non-fibrotic specimens from metastatic colorectal cancer and benign liver diseases who underwent percutaneous core liver biopsy, liver resection and liver transplantation at Koç University Hospital and Medipol University Hospital. Samples and clinical data were obtained under conditions of informed consent and upon approval of a local Institutional Review Board (2015.053.IRB1.014, 2016.024.IRB2.005, 2017.139.IRB2.048). The study protocol conforms to the ethical guidelines of the 1975 Declaration of Helsinki. Written informed consent obtained from patients or relatives (legal guardians) in accordance with Declaration of Helsinki.

Animal materials

To test the imaging method, a high fat high sucrose diet (HFHS) and Carbon tetrachloride (CCl₄) -induced mouse MASLD model was utilized which resembles the model established by Tsuchida et al. by combination of the hepatotoxin and dietary manipulation³⁵. Compared to HFHS or ALIOS (The American lifestyle-induced obesity syndrome diet)³⁶ alone, this animal model can generate a robust amount of fibrosis. On the contrary, CCl₄ and MCD (methionine-choline deficient diet) alone models are able to produce fibrosis and cirrhosis without recapitulating the metabolic features of MASLD. The MCD model can generate significant amounts of steatosis, however, resulting in up to 30% weight loss. A total of 48 male C57Bl6/J mice were fed high fat high sucrose diet (HFHS) and Carbon tetrachloride (CCl₄) or HFHS and olive oil for 6, 9 and 12 weeks (Research Diets, New Jersey, USA). Histological features of MASLD were induced with the administration of CCl₄ intraperitoneally in olive oil (1:3) at a dosage of 0.2 µl/g. At the end of the weeks, mice were euthanized using overdose of isoflurane inhalation. The chest cavity was opened followed by perfusion with modified

hydrogel monomer solution (HM solution). Livers were harvested and used for the modified CLARITY. All study protocols were approved by the Institutional Animal Care and Use Committee (IACUC) of Koç University with approval number 2015.HADYEK.003/009 according to Directive 2010/63/EU of the European Parliament and the Council on the Protection of Animals Used for Scientific Purposes. Animal experiments and the study were reported in accordance with the ARRIVE guidelines. All methods were performed in accordance with the relevant guidelines and regulations.

Clarifying non-fibrotic and fibrotic liver specimens

To generate a 3D imaging platform for hepatic ECM components, firstly, tissue clarification technique (CLARITY) was applied to human liver tissues²¹. Liver samples over 10 mm in length were chosen for staining as well as clinical criteria's for MASLD or Viral induced fibrosis. CLARITY method consists of the following brief steps: (i) fixation of tissues with paraformaldehyde and hydrogel embedding; (ii) membrane lipid removal by clearing buffer containing 200 nM boric acid and 4% sodium dodecyl sulphate (SDS) in distilled water; (iii) refractive index homogenisation; (iv) molecular labelling with fluorescent antibodies (Supplementary Material and Method). Accordingly, fresh liver tissues were fixed by cross-linking with paraformaldehyde. Hydrogel monomers were infused into the liver tissue and cross-linked with tissue proteins. Formalin-fixed paraffin-embedded liver samples were deparaffinized by heating and Xylene/ethanol application. Subsequently, translucent lipid bilayers were removed by detergents while leaving cross-linked biomolecules intact (Fig. 1A, Supplementary Fig. S5)²¹. Given that performance of tissue clearing techniques has not been previously shown in dense fibrotic tissues, different concentrations of hydrogel embedding and clearing solutions were tested and adjusted based on the previously published methods²¹. To identify optimal clearing conditions, we examined different acrylamide and bisacrylamide concentrations according to the size and fibrosis content of the specimen (Supplementary Table S4, Supplementary Material and Method). Adjustment of bisacrylamide concentration in monomer solution resulted in increased transparency and tissue integrity of core biopsy specimens. Therefore, resected healthy liver tissues, liver biopsy samples and explant cirrhotic tissues were passively clarified by an optimized protocol (Fig. 1B–D). Tissues became progressively clearer and full transparency was achieved even in advanced cirrhotic tissues as shown in Fig. 1D.

Staining of cleared human liver tissues

Clarified liver tissues were incubated with anti-Collagen type I (1:2500 Abcam, Cambridge, UK) and Elastin antibodies (1:2500, Merck Millipore, Massachusetts, USA) in Phosphate Buffer Saline-Tween20 (PBSTw, with 0.1% (vol/vol) Tween-20) with 0.01% (wt/vol) sodium azide at + 4 °C with gentle agitation. and washed in PBSTw (0.01% (vol/vol) Tween-20), then exposed to 5% goat serum (Cell Signalling, Massachusetts, USA) to reduce non-specific binding. Samples were incubated with CY3-conjugated secondary antibodies (1:500, Jackson ImmunoResearch, Philadelphia, PA). Nucleus staining was performed overnight with Hoechst solution (1:1000, Thermo Scientific, Vienna, Austria) in PBS. After excess solutions were washed off, samples were incubated in refractive index matching solution.

LSM imaging

We established a custom-made in-house developed light-sheet microscopy (LSM) based on the OpenSPIM platform which enables us to perform high-resolution 3D imaging with a high image acquisition rate³⁷. The optical system mainly included a cylindrical lens which generates a static light-sheet, illumination sources of solid-state diode lasers, a polarising beam splitter and a CMOS (complementary metal-oxide-semiconductor) image sensor (Fig. 1E, Supplementary Fig. S6). Total magnification is chosen as 7.5X for imaging a large FOV and high throughput. In this configuration, the system has a Full Width Half Maximum (FWHM) of 23 µm in the axial (Z) direction and a FWHM of 3.5 µm in the lateral (XY) plane (Supplementary Fig. S6C). Tissues were embedded in a mixture of low melting agarose and a Refractive index matching solution (RIM) solution (RI of 1.45) in borosilicate tubes (Axis-Shield, Norway) (Supplementary Fig. S5). The RIM solution RI must match with RI of cleared samples, otherwise blurry images would be acquired. The tubes were horizontally placed in a glycerol-filled sample cage. Images were acquired as the Z-step size would be 2–10 µm by glycerol-dipping objectives and reconstructed into 3D volumetric images and videos (Fig. 1F).

Image analysis and quantification

Quantification of fibrosis was performed by collagen proportionate area (CPA) analysis approach using computerised macro code with ImageJ (Supplementary Material and Method). Hundreds of visualized sections were analyzed to assess fibrosis generating CPV and EPV values for each patient. CPV and EPV values were calculated by averaging CPA and EPA values of each sample.

Statistical analysis

Cut-off values for CPA/CPV/EPV were established by calculating the area under receiver operator (AUROC) curves and using the Youden index. Interquartile range (IQR) was measured for all fibrotic stages. 3D histogram analysis executed by MATLAB R2021b (The MathWorks, Inc.). The significance level was set to be at 0.05 or lower. (* $p \leq 0.05$, ** $p \leq 0.01$, *** $p \leq 0.001$)

Data availability

The datasets generated and analysed during this study are available from the corresponding author on reasonable request.

Received: 7 November 2024; Accepted: 14 April 2025

References

- Friedman, S. L. & Pinzani, M. Hepatic fibrosis 2022: Unmet needs and a blueprint for the future. *Hepatology* **75**, 473–488. <https://doi.org/10.1002/hep.32285> (2022).
- Younossi, Z. et al. Global burden of NAFLD and NASH: Trends, predictions, risk factors and prevention. *Nat. Rev. Gastroenterol. Hepatol.* **15**, 11–20. <https://doi.org/10.1038/nrgastro.2017.109> (2018).
- Riazi, K. et al. The prevalence and incidence of NAFLD worldwide: A systematic review and meta-analysis. *Lancet Gastroenterol. Hepatol.* **7**, 851–861. [https://doi.org/10.1016/s2468-1253\(22\)00165-0](https://doi.org/10.1016/s2468-1253(22)00165-0) (2022).
- Angulo, P. et al. Liver fibrosis, but no other histologic features, is associated with Long-term outcomes of patients with nonalcoholic fatty liver disease. *Gastroenterology* **149**, 389–397e310. <https://doi.org/10.1053/j.gastro.2015.04.043> (2015).
- Ekstedt, M. et al. Fibrosis stage is the strongest predictor for disease-specific mortality in NAFLD after up to 33 years of follow-up. *Hepatology* **61**, 1547–1554. <https://doi.org/10.1002/hep.27368> (2015).
- Tang, A. et al. Comparative burden of metabolic dysfunction in lean NAFLD vs Non-lean NAFLD—A systematic review and Meta-analysis. *Clin. Gastroenterol. Hepatol.* **21**, 1750–1760e1712. <https://doi.org/10.1016/j.cgh.2022.06.029> (2023).
- Jamialahmadi, O. et al. Partitioned polygenic risk scores identify distinct types of metabolic dysfunction-associated steatotic liver disease. *Nat. Med.* **30**, 3614–3623. <https://doi.org/10.1038/s41591-024-03284-0> (2024).
- Standish, R. A., Cholongitas, E., Dhillon, A., Burroughs, A. K. & Dhillon, A. P. An appraisal of the histopathological assessment of liver fibrosis. *Gut* **55**, 569–578. <https://doi.org/10.1136/gut.2005.084475> (2006).
- Bedossa, P. Utility and appropriateness of the fatty liver Inhibition of progression (FLIP) algorithm and steatosis, activity, and fibrosis (SAF) score in the evaluation of biopsies of nonalcoholic fatty liver disease. *Hepatology* **60**, 565–575. <https://doi.org/10.1002/hep.27173> (2014).
- Davison, B. A. et al. Suboptimal reliability of liver biopsy evaluation has implications for randomized clinical trials. *J. Hepatol.* **73**, 1322–1332. <https://doi.org/10.1016/j.jhep.2020.06.025> (2020).
- The French METAVIR Cooperative Study Group. Intraobserver Interobserver variations in liver biopsy interpretation in patients with chronic hepatitis C. *Hepatology* **20**, 15–20 (1994).
- Ratziu, V. et al. Sampling variability of liver biopsy in nonalcoholic fatty liver disease. *Gastroenterology* **128**, 1898–1906. <https://doi.org/10.1053/j.gastro.2005.03.084> (2005).
- Ratziu, V. & Friedman, S. L. Why do so many nonalcoholic steatohepatitis trials fail? *Gastroenterology* **165**, 5–10. <https://doi.org/10.1053/j.gastro.2020.05.046> (2023).
- Calvaruso, V. et al. Computer-assisted image analysis of liver collagen: relationship to Ishak scoring and hepatic venous pressure gradient. *Hepatology* **49**, 1236–1244. <https://doi.org/10.1002/hep.22745> (2009).
- Buzzetti, E. et al. Collagen proportionate area is an independent predictor of long-term outcome in patients with non-alcoholic fatty liver disease. *Aliment. Pharmacol. Ther.* **49**, 1214–1222. <https://doi.org/10.1111/apt.15219> (2019).
- Tsochatzis, E. et al. Collagen proportionate area is superior to other histological methods for sub-classifying cirrhosis and determining prognosis. *J. Hepatol.* **60**, 948–954. <https://doi.org/10.1016/j.jhep.2013.12.023> (2014).
- Gailhouste, L. et al. Fibrillar collagen scoring by second harmonic microscopy: A new tool in the assessment of liver fibrosis. *J. Hepatol.* **52**, 398–406. <https://doi.org/10.1016/j.jhep.2009.12.009> (2010).
- Wang, Y. et al. Quantifying and monitoring fibrosis in non-alcoholic fatty liver disease using dual-photon microscopy. *Gut* **69**, 1116–1126. <https://doi.org/10.1136/gutjnl-2019-318841> (2020).
- Segovia-Miranda, F. et al. Three-dimensional spatially resolved geometrical and functional models of human liver tissue reveal new aspects of NAFLD progression. *Nat. Med.* **25**, 1885–1893. <https://doi.org/10.1038/s41591-019-0660-7> (2019).
- Richardson, D. S. & Lichtman, J. W. Clarifying tissue clearing. *Cell* **162**, 246–257. <https://doi.org/10.1016/j.cell.2015.06.067> (2015).
- Chung, K. & Deisseroth, K. CLARITY for mapping the nervous system. *Nat. Methods.* **10**, 508–513. <https://doi.org/10.1038/nmeth.2481> (2013).
- Ertürk, A. et al. Three-dimensional imaging of solvent-cleared organs using 3DISCO. *Nat. Protoc.* **7**, 1983–1995. <https://doi.org/10.1038/nprot.2012.119> (2012).
- Nojima, S. et al. CUBIC pathology: Three-dimensional imaging for pathological diagnosis. *Sci. Rep.* **7**, 9269. <https://doi.org/10.1038/s41598-017-09117-0> (2017).
- Tomer, R., Ye, L., Hsueh, B. & Deisseroth, K. Advanced CLARITY for rapid and high-resolution imaging of intact tissues. *Nat. Protoc.* **9**, 1682–1697. <https://doi.org/10.1038/nprot.2014.123> (2014).
- Yilmaz, Y. et al. TASL practice guidance on the clinical assessment and management of patients with nonalcoholic fatty liver disease. *Hepatol. Forum* **4**, 1–32. <https://doi.org/10.14744/hf.2023.2023.0011> (2023).
- Yilmaz, Y. The heated debate over NAFLD renaming: An ongoing saga. *Hepatol. Forum* **4**, 89–91. <https://doi.org/10.14744/hf.2023.2023.0044> (2023).
- Kawamura, N. et al. Influence of liver stiffness heterogeneity on staging fibrosis in patients with nonalcoholic fatty liver disease. *Hepatology* **76**, 186–195. <https://doi.org/10.1002/hep.32302> (2022).
- Rezvani Habibabadi, R. et al. Comparison between ROI-based and volumetric measurements in quantifying heterogeneity of liver stiffness using MR elastography. *Eur. Radiol.* **30**, 1609–1615. <https://doi.org/10.1007/s00330-019-06478-0> (2020).
- Sanyal, A. J. et al. The natural history of advanced fibrosis due to nonalcoholic steatohepatitis: data from the Simtuzumab trials. *Hepatology* **70**, 1913–1927. <https://doi.org/10.1002/hep.30664> (2019).
- Malik, A. H. et al. Correlation of percutaneous liver biopsy fragmentation with the degree of fibrosis. *Aliment. Pharmacol. Ther.* **19**, 545–549. <https://doi.org/10.1111/j.1365-2036.2004.01882.x> (2004).
- Glaser, A. K. et al. Light-sheet microscopy for slide-free non-destructive pathology of large clinical specimens. *Nat. Biomed. Eng.* <https://doi.org/10.1038/s41551-017-0084> (2017).
- Liu, J. T. C. et al. Harnessing non-destructive 3D pathology. *Nat. Biomed. Eng.* **5**, 203–218. <https://doi.org/10.1038/s41551-020-00681-x> (2021).
- Tanaka, N. et al. Whole-tissue biopsy phenotyping of three-dimensional tumours reveals patterns of cancer heterogeneity. *Nat. Biomed. Eng.* **1**, 796–806. <https://doi.org/10.1038/s41551-017-0139-0> (2017).
- Serafin, R., Xie, W., Glaser, A. K. & Liu, J. T. C. FalseColor-Python: A rapid intensity-leveling and digital-staining package for fluorescence-based slide-free digital pathology. *PLoS One.* **15**, e0233198. <https://doi.org/10.1371/journal.pone.0233198> (2020).
- Tsuchida, T. et al. A simple diet- and chemical-induced murine NASH model with rapid progression of steatohepatitis, fibrosis and liver cancer. *J. Hepatol.* **69**, 385–395. <https://doi.org/10.1016/j.jhep.2018.03.011> (2018).
- Tetri, L. H., Basaranoglu, M., Brunt, E. M., Yerian, L. M. & Neuschwander-Tetri, B. A. Severe NAFLD with hepatic necroinflammatory changes in mice fed trans fats and a high-fructose corn syrup equivalent. *Am. J. Physiol. Gastrointest. Liver Physiol.* **295**, G987–G995. <https://doi.org/10.1152/ajpgi.90272.2008> (2008).
- Pitrone, P. G. et al. OpenSPIM: An open-access light-sheet microscopy platform. *Nat. Methods* **10**, 598–599. <https://doi.org/10.1038/nmeth.2507> (2013).

Acknowledgements

The authors would like to thank Ms Simal Lacin for technical assistance, Dr Arzu Baygul for statistical support and Mr. Batuhan Alpdogan for his assistance with the image processing. This project is supported by Scientific and Technological Research Council of Turkey (TUBITAK) 1001 grant with a project number of 117S440. A. Kiraz acknowledges partial support from the Turkish Academy of Sciences (TUBA). The authors gratefully acknowledge the use of the services and facilities of the Koç University Research Center for Translational Medicine (KUTTAM), equally funded by the Republic of Turkey Ministry of Development Research Infrastructure Support Program. Findings, opinions, or points of view expressed in this article do not necessarily represent the official position or policies of the Ministry of Development.

Author contributions

M.Z. designed the study, interpreted data, and drafted the manuscript. B.Y. performed acquisition, image processing, statistical analysis and interpretation of majority of the data for the manuscript. M.Z., M.D., M.A., G.T., C.Y., M.E. recruited the patients to the study. B.Y., T.S., E.O., Y.U. and O.Y. performed the 3D imaging. B.U., A.S., D.A., E.D. and G.P.A. performed analysis and interpretation of the data. A.K., B.M., Y.G.O, S.K., Y.C.T., M.A. supervised the imaging experiments, and LSM configuration. H.K. performed histopathological analysis and staging. O.F. supervised the analysis of the volumetric images. M.A. designed the automated code for imaging with LSM. All authors reviewed the manuscript critically for important intellectual content.

Declarations

Competing interests

The authors declare no competing interests.

Additional information

Supplementary Information The online version contains supplementary material available at <https://doi.org/10.1038/s41598-025-98680-y>.

Correspondence and requests for materials should be addressed to M.Z.

Reprints and permissions information is available at www.nature.com/reprints.

Publisher's note Springer Nature remains neutral with regard to jurisdictional claims in published maps and institutional affiliations.

Open Access This article is licensed under a Creative Commons Attribution-NonCommercial-NoDerivatives 4.0 International License, which permits any non-commercial use, sharing, distribution and reproduction in any medium or format, as long as you give appropriate credit to the original author(s) and the source, provide a link to the Creative Commons licence, and indicate if you modified the licensed material. You do not have permission under this licence to share adapted material derived from this article or parts of it. The images or other third party material in this article are included in the article's Creative Commons licence, unless indicated otherwise in a credit line to the material. If material is not included in the article's Creative Commons licence and your intended use is not permitted by statutory regulation or exceeds the permitted use, you will need to obtain permission directly from the copyright holder. To view a copy of this licence, visit <http://creativecommons.org/licenses/by-nc-nd/4.0/>.

© The Author(s) 2025